Normalized Hodographic Mapping for Constrained Trajectory Families

FANG TOH SUN*
Massachusetts Institute of Technology, Cambridge, Mass.

A special method of hodographic mapping for families of constrained trajectories is presented. A nondimensional velocity space is introduced, and the complexity of a family of infinite Keplerian trajectories under given constraints is reduced by such a mapping to the simple geometry of a unit circle and a characteristic curve or surface in this vector space. The latter plays the dual role of being the locus of the hodograph origin on the one hand, and the eccentricity indicatrix of the family on the other hand. It, together with the unit circle, constitutes the normalized hodograph image of the entire family. The fundamental concepts and principles underlying this mapping are outlined. A set of rules which enable one to observe the global characteristics of the family and those of its particular trajectories from its normalized hodograph image is developed. A number of Keplerian trajectory families under typical constraints are mapped. Applications of such a mapping to the solution of trajectory problems are illustrated with examples. To facilitate the analytic treatment, and to provide quick graphic solutions, a set of normalized hodographic maps is presented.

I. Introduction

IN space-flight problems one often needs to investigate the totality of a class of trajectories all satisfying certain common constraints. Such trajectory families arise in mission planning, trajectory optimization, and many other problems, and their global analyses are often indispensable prior to the selection of a particular trajectory to suit the purpose. Unfortunately, the complexity of the geometry of a trajectory family in the position space, even in the simple case as Kepler motion, usually makes the analytic treatment prohibitive. As generally known, the classic hodographic mapping has the advantage of transforming a Kepler conic into a circle in the velocity space.[1,5,7,9] Though considerable simplification results from such mapping when one or few Keplerian trajectories are involved, it is not yet enough in the presence of a family of infinitely many Keplerian trajectories. To render further simplification, the method of normalized hodographic mapping is found of great help. This special method of mapping is in line with Hamilton's circular hodograph.[1] It was first introduced in Ref. 5 and later applied to the two-terminal trajectory analysis.[6] The present paper intends to give, for the first time, a systematic presentation of the fundamental concepts and principles underlying such a mapping, illustrated with the mapping of a number of typically constrained trajectory families of frequent occurrence and several examples of practical applications. It will be shown that such a mapping not only greatly facilitates the analytic treatment of trajectory families, but, in many cases, it may lead directly to the solution of the problem.

II. Basic Concepts of Normalized Hodographic Mapping

The normalized velocity vector $\boldsymbol{v}$ for the motion in a Newtonian gravity field is defined by

$$\boldsymbol{v} = h\dot{\mathbf{r}}/\mu \tag{1}$$

where h is the scalar angular momentum per unit orbiting mass; μ the strength of the Newtonian field; $\mathbf{r}$ the position vector; and the dot indicates differentiation with respect to time. It is to be noted that h here is constant along a trajectory, but varies from one trajectory to another. This aspect distinguishes the present normalization from the usual nondimensionalization by referring to an absolute constant. In the following we will assume $h > 0$ unless otherwise stated. As shown in Ref. 5, through such a normalization, the Hamiltonian hodograph for any Kepler conic in the $\mathbf{r}$-space reduces to a unit circle in the $\boldsymbol{v}$-space. Consequently, a family of Keplerian trajectories will be mapped onto a family of unit circles if the origin of the $\boldsymbol{v}$-space is fixed. However, to attain further simplification we will consider the center of the hodograph circle fixed instead and let the origin of the hodograph vary. Thus, associated with each particular trajectory in the $\mathbf{r}$-space, there is a particular origin O in the $\boldsymbol{v}$-space. The totality of these points constitutes the locus of the hodograph origins, which will be called the O-locus. The hodograph of all coplanar Keplerian trajectories are thus mapped onto the same unit circle, which, together with the O-locus, constitutes the image of the entire family in the $\boldsymbol{v}$-space. For a spatial family, the unit circle generates a unit hodograph sphere.

In essence the normalized hodographic mapping as outlined above is a curve-to-point transformation.[2] Such a mapping is, in general, not one-to-one, since all homothetic Kepler conics will be mapped into the same point in the $\boldsymbol{v}$-space. However, if we confine our attention to the class of families all members of which pass through a fixed point in the $\mathbf{r}$-space (Fig. 1), the mapping will be one-to-one, except at some singular points. Such coterminal families are the ones usually encountered in trajectory problems, and the following treatment will be confined to this class. The common point Q_0 defined by its position vector $\mathbf{r}_0$ (r_0 being finite) may be regarded as the initial point of all trajectories of the family, though it need not be so. It can be easily seen that such coterminal trajectories form a family of Kepler conics of ∞^3 extent, and hence its O-locus is at most 3 dimensional. With the presence of N (≤ 3) additional independent constraint equations, the family will reduce to ∞^{3-N} extent, with a $(3-N)$-dimensional O-locus. Thus, with $N = 1$, the locus is a 2-dimensional surface in the 3-dimensional $\boldsymbol{v}$-space; and with $N = 2$, it is a curve, which will be planar if the trajectory family is planar.

Presented as Paper 69-924 at the AIAA/AAS Astrodynamics Conference, Princeton, N.J., August 20–22, 1969; submitted September 16, 1969; revision received August 3, 1970. This work was done at NASA Electronic Research Center, Cambridge, Mass.

* Senior Research Associate, NAS-NRC, presently with the Department of Mathematics. Member AIAA.

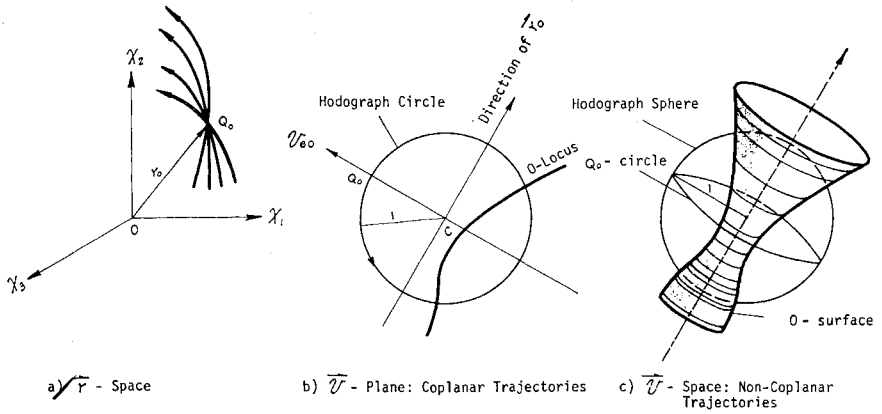

Fig. 1 The coterminal Keplerian trajectory family and its normalized hodograph image.

III. Essential Trajectory Information Derived from the Normalized Hodograph

To obtain trajectory information from the normalized hodograph we call particular attention to the triangle OCQ_O (Fig. 2), which contains all the basic information concerning the trajectory through Q_O, associated with the origin point O (Q_O in the $\mathbf{v}$ space is the image of Q_O in the $\mathbf{r}$ space; C is the center of the hodograph circle). 1) The three vectors forming the triangle have the significances:

$$\mathbf{OQ}_O = \mathbf{v}_O\mathbf{OC} = \boldsymbol{\varepsilon} \qquad \mathbf{CQ}_O = \mathbf{e}_{\theta O} \tag{2}$$

where $\mathbf{v}_O$ is the normalized velocity at Q_O, defined by Eq. (1); $\boldsymbol{\varepsilon}$ is the eccentricity vector, defined as the vector in the direction of the lateral axis of the trajectory conic, with its length equal to the numerical eccentricity; and $\mathbf{e}_{\theta O}$ is a unit vector in the local transversal direction of motion. 2) The three interior angles of the triangle give the three angular variables at Q_O, the true anomaly θ_O, and the path angles ϕ_O and β_O with reference to the local horizon and apsidal axis, respectively, as follows:

$$\angle OCQ_O = \pi - \theta_O, \quad \angle CQ_OO = \phi_O, \quad \angle COQ_O = \beta_O - \pi/2 \tag{3}$$

From such basic observation, other trajectory information may be readily derived. For convenience we attach a pair of rectangular axes, ξ and η, to Q_O (Fig. 2b) and observe the following. 3) The coordinates (ξ,η) of the point O give the transversal and radial components of

$$\mathbf{v}_{\theta O} = \xi\mathbf{e}_{\theta O} \qquad \mathbf{v}_{rO} = -\eta\mathbf{e}_{rO} \tag{4}$$

4) The abscissa ξ alone of the point O defines the angular momentum h and the semilatus rectum $\bar{r}$ of the trajectory in accordance with

$$h = (\mu r_O\xi)^{1/2} \qquad \bar{r} = r_O\xi \tag{5}$$

5) The point B, where the line through O and normal to $\mathbf{v}_O$ crosses the ξ axis, defines the local speed ratios ν_O and λ_O at Q_O, the orbital energy k and the semimajor axis a as follows:

$$\nu_O^2 = 2\lambda_O^2 = \overline{BQ}_O \qquad k = -(\mu/2r_O)B\tilde{Q}_O \qquad a = r_O/B\tilde{Q}_O \tag{6}$$

where $\nu_O = V_O/V_s$, and $\lambda_O = V_O/V^*$ by definition, V_s and V^* being the circular and escape speeds at Q_O, respectively; $\tilde{Q}_O$ is the point on the hodograph circle, diametrically opposite to Q_O; and the directed line segment $B\tilde{Q}_O$ is positive in the direction of the ξ axis.

Additional information is given in the Appendix of Ref. 10. Before proceeding to the next section, two important remarks are in order. First, while the vector $\mathbf{OQ}_O$ gives the correct direction of the trajectory velocity $\mathbf{V}_O$, its length is not equal to the scalar speed V_O. However, with h given by Eq. (5), the evaluation of V_O by Eq. (1) is straightforward. Alternately, the first of Eqs. (6) also enables one to determine V_O by first evaluating ν_O or λ_O. Second, in view of the fact that $\mathbf{OC} = \boldsymbol{\varepsilon}$, the O locus of a coterminal trajectory not only describes the normalized terminal velocities of the family, but also its eccentricity vectors. Hence the **O**-locus may be appropriately regarded as the eccentricity indicatrix of the family. A glance of the triangle OCQ_O shows that the two vectors, $\mathbf{v}_O$ and $\boldsymbol{\varepsilon}$ are simply related by

$$\mathbf{v}_O - \boldsymbol{\varepsilon} = \mathbf{e}_{\theta O} \tag{7}$$

where $\mathbf{e}_{\theta O}$ is constant for a fixed terminal point Q_O.

IV. Characteristics of the Trajectory Family and the Geometry of Its O Locus

Consider a planar coterminal family of the same sense of motion around the field center (say, counterclockwise, and designated as positive). We first note that the point Q_O in the $\mathbf{v}$-space is a singular point, since all rectilinear trajectories in the $\mathbf{r}$-space will be mapped into this same point, and the one-

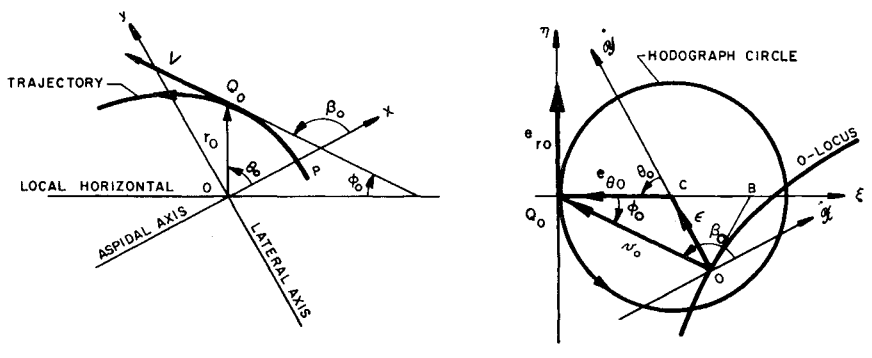

Fig. 2 Basic correlation between the Keplerian trajectory and its normalized hodograph image.

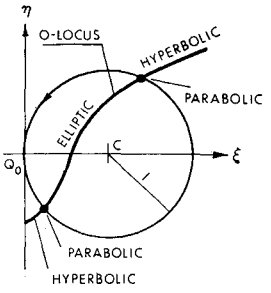

Fig. 3 The *O*-locus and the types of Keplerian conics in the trajectory family.

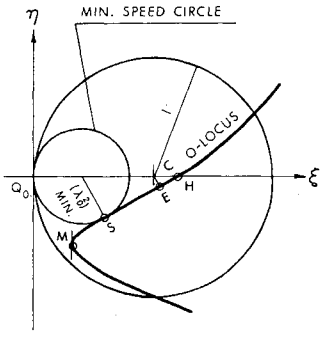

Fig. 4 The *O*-locus and the particular trajectories of the family.

M MIN. ANGULAR MOMENTUM TRAJECTORY
S MIN. ENERGY TRAJECTORY
E LEAST ECCENTRIC TRAJECTORY
H HORIZONTAL DEPARTURE

to-one correspondance fails there. At Q_O ($\xi = 0, \eta = 0$) we have $h = 0$, but the other parameters like V_O, k, etc. are indeterminate. The corresponding hodograph is no longer the unit circle, but degenerates into the point Q_O itself. This point requires special consideration whenever it appears on the O locus. It will be excluded in the following analysis unless otherwise stated. Second, with Q_O disposed, we must further restrict the O-locus to the half-plane $\xi > 0$ since a point on the η axis, where $\xi = 0, \eta \neq 0$, will necessarily associate Q_O with the trajectory point at infinity in the **r**-space, hence contradict the assumption that r_O is finite; and the points $\xi < 0$ are meaningless in a gravity field.[5,6] With these preliminary observations and the background information in Sec. III, the essential characteristics of the trajectory family may now be observed from the geometry of its O-locus as related to the unit hodograph circle (called C-circle for short) as follows:

1) On the types of the trajectory conics of the family: a) the trajectories of the family will be all elliptic or all hyperbolic according as its O-locus is entirely inside or outside the C circle; a family will consist of both elliptic and hyperbolic trajectories if its O-locus lies partly inside and partly outside the C-circle; b) a parabolic trajectory will be present in the family when the O-locus and the C circle have a common point (nonsingular); c) a circular trajectory will be present when and only when the O-locus passes through the center C; d) no rectilinear trajectory can be present unless the O locus passes through the point Q_O (Fig. 3).

2) The magnitudes of eccentricity and angular momentum and, hence, the semilatus rectum pertaining to the family will be bounded if the O locus is bounded in the right half-plane, $\xi \geq 0$; otherwise, they are unbounded. However, the departure speed and hence the orbital energy and the semimajor axis will be bounded under the more stringent condition that the O locus is bounded, and that some constant $\delta > 0$ exists such that $\xi \geq d$ at every regular point on the O-locus.

3) The least and most eccentric trajectories of the family, if any, are given by the points on the O locus, which are closest to, and farthest from the center C, respectively. The point on the O locus associated with a trajectory of local stationary ϵ is then provided by the foot of the perpendicular drawn from C to the O-locus (Fig. 4). Analytically, this orthogonality condition may be expressed as

$$(d\eta/d\xi)_O = (1 - \xi)/\eta \tag{8}$$

where $(d\eta/d\xi)_O$ is the slope of the O-locus.

4) The minimum and maximum angular-momentum trajectories of the family, if any, are given by the points on the O-locus, which are nearest and farthest from the ξ-axis (Fig. 4). Thus a trajectory of local stationary h of the family is given by the point on the O-locus, where it has a vertical tangent, that is, $(d\xi/d\eta)_O = 0$. Obviously, an extremal h also implies an extremal $\bar{r}$ of the same nature.

5) The minimum and maximum energy trajectories of the family, if any, are given by the points on the O-locus, where pass the smallest and largest speed circles, respectively. (By "speed circle" we mean the circle of radius λ_O^2 and tangent to the C-circle internally at Q_O; see Fig. 4 and Ref. 5.) Analytically, it can be shown that the trajectory of stationary k of the family is given by the point on the O locus, where

$$(d\eta/d\xi)_O = (\eta^2 - \xi^2)/2\xi\eta \tag{9}$$

which is, in fact, the condition of tangency of the O-locus to a speed circle (Fig. 4). The extremity or stationarity of either one of k, a, and V_O implies the same of the other two, of course.

6) The point $H(\xi_O, 0)$, where the O-locus crosses the ξ axis, defines a trajectory of horizontal departure making Q_O the apoapsis if $\xi_O < 1$, or the periapsis if $\xi_O > 1$. If, in addition, the O-locus cuts the ξ axis orthogonally, then the parameters, ϵ, h, r, k, a, and V_O, pertaining to the family, will all reach their stationary values on the same trajectory defined by H (Fig. 4).

7) The directions of the apsidal axes pertaining to the family will be unrestricted if the O locus encloses the center C; otherwise, they will be restricted, and the limiting directions are defined by the outmost rays emanated from C, and being

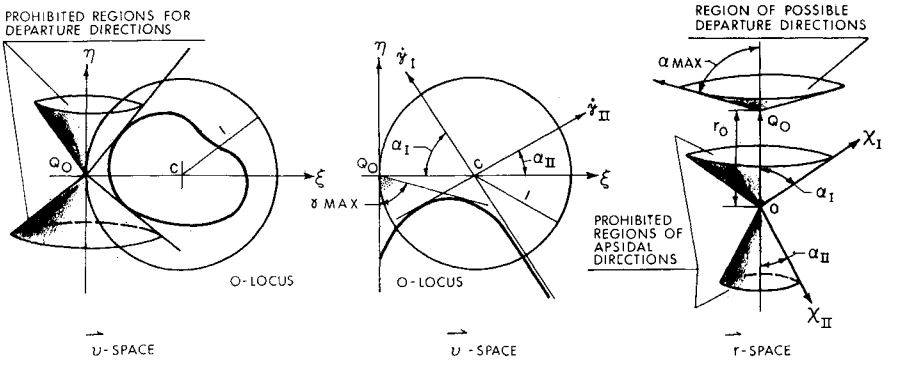

Fig. 5 The *O*-locus and the limiting directions.

(a) DEPARTURE DIRECTIONS LIMITED; APSIDAL DIRECTIONS UNLIMITED

(b) DEPARTURE DIRECTIONS AND APSIDAL DIRECTIONS BOTH LIMITED

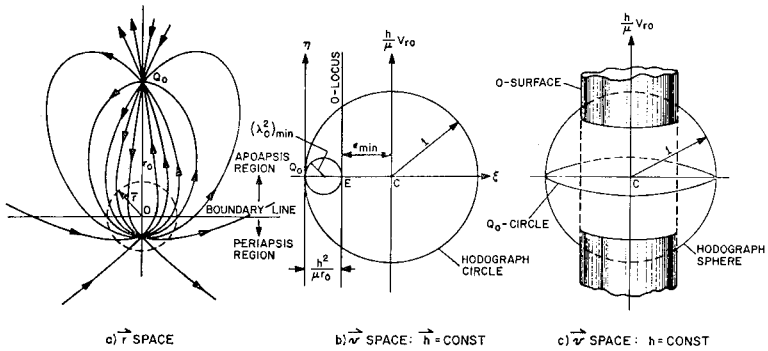

Fig. 6 The isoangular-momentum family of Keplerian trajectories.

a) a tangent to the O-locus, or b) its asymptote, or c) through an endpoint of it (Fig. 5). Whenever such limiting directions exist, there exist in the **r**-plane regions where the periapses and apoapses are confined.

8) Limiting directions of departure at Q_O always exist for a planar family of unisense, and they are defined by the outmost rays emanated from the point Q_O and being one of the class of lines enumerated under Item 7 (Fig. 5). Maximum directional bounds are given by $|\phi_O| < \pi/2$ when the O locus meets or tends to the positive and negative η axis.

So far we have restricted the trajectory family to be planar and of unisense. It can be easily seen that the hodograph images of two trajectory families under identical constraints, but of opposite senses, are mutual reflections in the center point C. Hence, once a family of positive sense is mapped, the hodograph image of its counterpart of the negative sense can readily be obtained. If the orientation of the plane of motion is not restricted, the planar family will become a spatial one in the **r**-space. The C-circle in the v-space will then generate a **C**-sphere, and the image point Q_O will move around C on its horizontal great circle. Consequently, the plane curve of the O-locus will generate a surface of revolution about the vertical axis through C (Fig. 1C). The directional regions in the plane, if exist, will generate limiting conical regions in space (Fig. 5). However, the hodograph images of the family in all planes are in fact identical, and all the foregoing assertions concerning a planar family hold in any arbitrary plane. Additional observations will be made after the mapping of some particular trajectory families is affected.

V. Normalized Hodographic Mapping of Typical Constrained Trajectory Families

By applying the fundamentals outlined in the preceding sections, eight families of Keplerian trajectories under typical constraints have been mapped and analyzed as summarized in Table 1 and graphically shown in Figs. 6 to 13. In each of these families one common terminal point Q_O in the **r**-space, and a positive sense of motion have been assumed. The details are given in the preprint,[10] and a few remarks ar given below:

1) Limiting apsidal directions exist in most of the families mapped (e.g. A, C, F, and H), and hence corresponding forbidden regions for the apses exist in the **r**-space. For example, in the equi-periapsis-radius family (r_P = const), the apsidal direction is limited by the two asymptotic directions of the O-locus (a branch of hyperbola), including an angle 2α, given by

$$\sin\alpha = r_P/r_O \tag{10}$$

and in the **r**-space, a portion of the spherical surface of radius r_P is unreachable for the periapses of the family (Fig. 11). No such limitation exists in an equi-apoapsis-radius family. However, limiting apsidal directions do exist in an isoenergetic family when the initial speed is below or equal to the local circular speed (Fig. 7) and in an isoeccentric hyperbolic family (Fig. 9).

2) Unrealistic trajectories may arise in a two-terminal family, and the corresponding points on the O-locus must be excluded (an unrealistic trajectory is the one having a point at infinity interposed between the two terminal points in the assumed sense of motion).[6] Such reality consideration necessarily restricts the linear locus of a two-terminal family to the semi-infinite line $O_I{}^*$ to ∞ for a range angle $\leq\pi$, or the finite segment $O_{II}{}^*T$ for a range angle $\geq\pi$ each being open at its both ends, and $O_I{}^*$ and $O_{II}{}^*$ are the two critical points, where the O line crosses the C circle.

3) The geometry of the normalized hodographs reveals a few characteristics of the trajectory families and simple relations, which are worth notice, as follows: a) Corresponding to a fixed direction of departure within the directional limits, there exists a pair of cotangential ellipses of the same eccentricity; their departure speeds are connected by

$$\lambda^2{}_{OI} + \lambda^2{}_{OII} = 1 \tag{11}$$

The two ellipses become coincident on the limiting direction, and we have $\lambda_O{}^2 = \frac{1}{2}$, that is, departure at circular speed. No such isoeccentric cotangential pair is possible in the parabolic or hyperbolic case. b) In an isoeccentric family (ϵ = const), the two oblique velocity components, V_Θ and V_Y, in

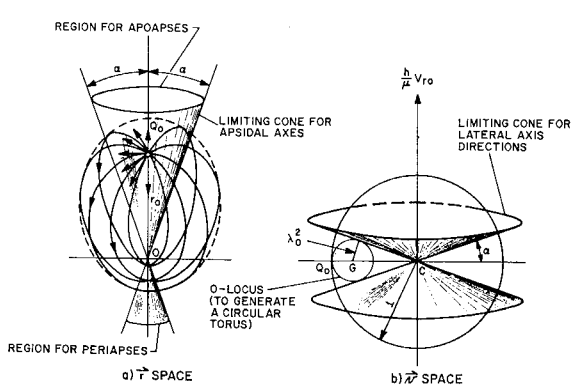

Fig. 7 The isoenergetic family of Keplerian trajectories.

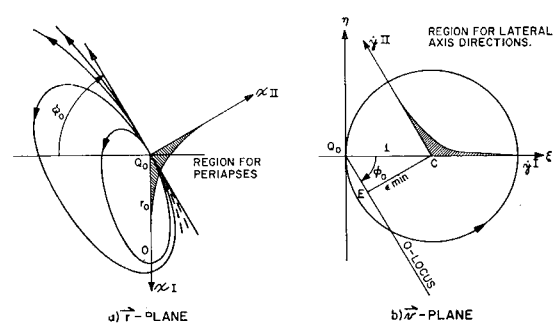

Fig. 8 The cotangential family of Keplerian trajectories.

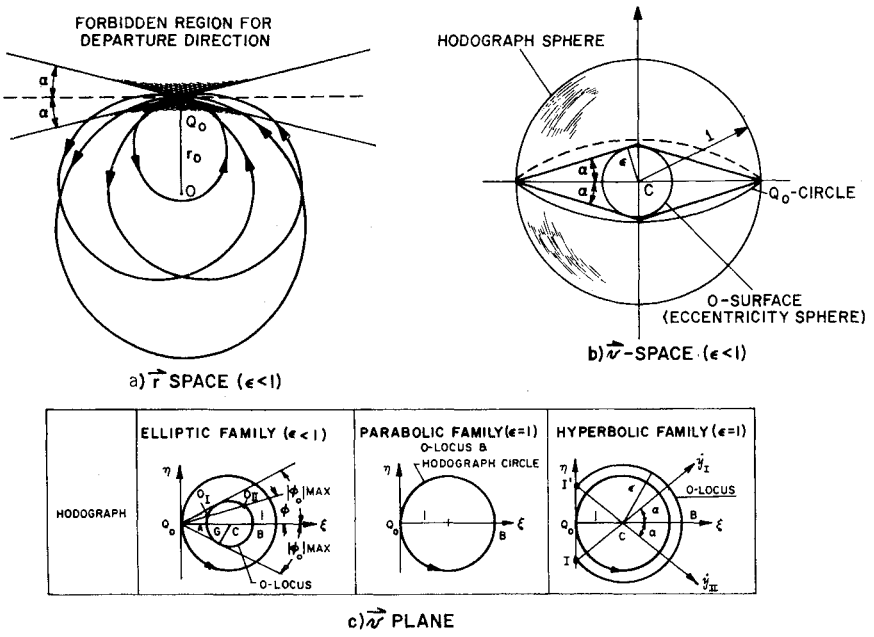

Fig. 9 The isoeccentric family of Keplerian trajectories.

the transversal and lateral axial directions respectively bear the constant ratio

$$V_T/V_\Theta = \epsilon \tag{12}$$

at any orbital point throughout the family. They are the invariant velocity components[9] along a Kepler conc, but in general, vary from one Kepler conic to another. c) In a coaxial family (θ_O = const, Fig. 10), we have the particular relation

$$V_{RO}V_{TO} = -(\mu/r_O)\tan\theta_O \sec\theta_O \tag{13}$$

where V_{RO} and V_{TO} are the components of the terminal velocity in the radial and lateral directions, respectively. Equation (13) shows that the product of these two components (generally nonorthogonal) is a constant, which depends on the fixed axial direction only, but independent of the particular choice of the trajectory. d) In a two-terminal family, all the peakpoints along different trajectories connecting the same two terminal points in the same sense of motion are located on the same radial line through the field center. (By "peakpoint" we mean the highest point on the trajectory above the line of sight.) This is a direct consequence of the linear O locus. For details and other consequences see Refs. 6 and 10.

4. Trajectories of various extremal parameters are found to exist in all the families mapped. Such are usually the subjects of interest in mission planning and trajectory optimization; relevant information is provided in Ref. 10.

VI. Additional Information on the Characteristics of a Trajectory Family

In the light of the mapping of the trajectory families F, G and H, additional observations in supplement to Sec. IV are now in order.

1) The existence of O-hyperbolas in the v-space enables one to find the particular member of a trajectory family that has the smallest or the largest periapsis radius, if any, by finding the O-hyperbola of the highest or the lowest σ_p respectively, that passes through the O-locus of the family. The same statement applies also to finding the particular member of the smallest or the largest apoapsis radius of the family if we replace the O-hyperbola by the O-ellipse, and σ_P by σ_A. Noting that both the O-ellipse and the O-hyperbola may be represented by the same equation,

$$[(1+\sigma)\xi - 1]^2 + \eta^2(1+\sigma)/(1-\sigma) = 1 \tag{14}$$

where σ stands for either σ_A or σ_P, an analytic condition sufficient for a point O on the O locus to yield a trajectory of local stationary apsidal radius of the family is

$$\xi^2\eta(d\eta/d\xi)_0^2 - 2\xi(\eta^2 - \xi + 1)(d\eta/d\xi)_0 + \eta(\eta^2 - 2\xi + 1) = 0 \tag{15}$$

where $(d\eta/d\xi)_0$ is the slope of the O locus. Equation (15) actually expresses the condition of tangency of the O locus to

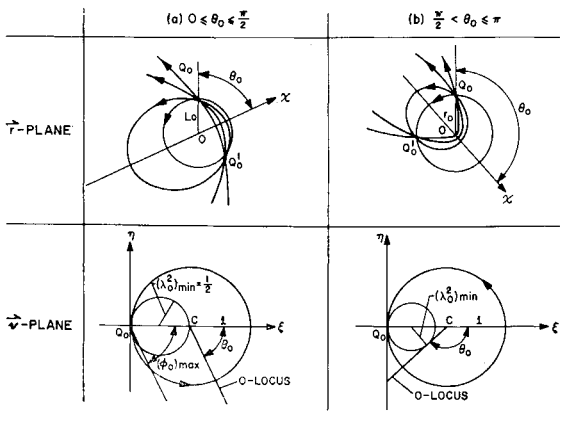

Fig. 10 The coaxial family of Keplerian trajectories.

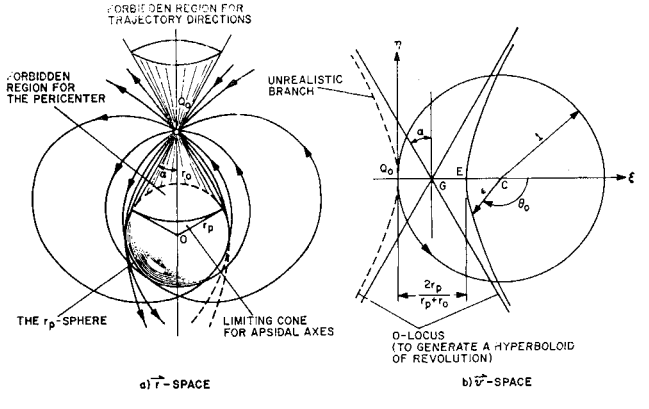

Fig. 11 The equiperiapsis-radius family of Keplerian trajectories.

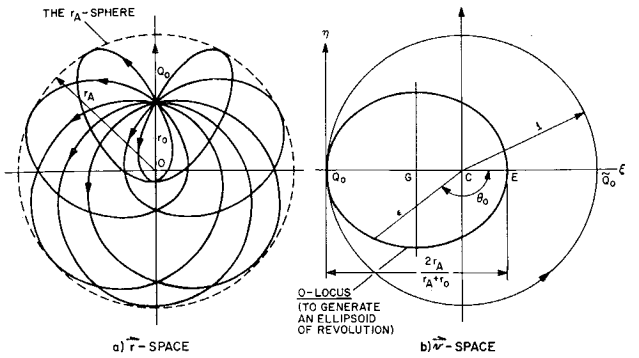

Fig. 12 The equiapoapsis-radius family of Keplerian trajectories.

the O-ellipse or the O-hyperbola, which, together with Eq. (14) and the equation of the O-locus, $f(\xi,\eta) = 0$ are sufficient to determine the values of ξ, η, and σ at the point O. The associated trajectory will have a stationary r_A if $\sigma < 1$, or a stationary r_P if $\sigma > 1$. When $\sigma = 1$ the O-ellipse or the O-hyperbola degenerates, so that the solution point is given by the ξ intercept of the O locus, and we have $(r_A)_{\min} = r_O$ if $\xi < 1$; $(r_P)_{\max} = r_O$ if $\xi > 1$; and $(r_A)_{\min} = (r_P)_{\max} = r_O$ if $\xi = 1$ (a circular orbit).

2) Noting that both the O-ellipse and the O-hyperbola are orthogonal to the ξ axis, condition (15) enables one to assert that, if the O locus of a family crosses the ξ axis orthogonally at $H(\xi_0,0)$ then the point H will define a trajectory of stationary apsidal radius of the family in accordance with

$$(r_A)_{\min} = r_O\xi_O/(2 - \xi_O) \text{ if } 1 \leq \xi_O < 2$$
$$(r_P)_{\max} = r_O\xi_O/(2 - \xi_O) \text{ if } 0 < \xi_O \leq 1 \tag{16}$$

3) It is sometimes of interest to know whether a second common point exists in a trajectory family in addition to the one assumed a priori. The mapping of the two-terminal family enables one to assert that no such a point is possible in a coterminal Keplerian family unless its O-locus is linear. Detailed discussion is found in Ref. 10.

VII. Examples of Applications

As a first example, we consider Roth's problem[8] of determining a trajectory between two position vectors $\mathbf{r}_1$ and $\mathbf{r}_2$ with a specified periapsis radius, $r_P^* \gtrless r_1$ or r_2. An analytic treatment by Roth is found in Ref. 8. In the following it will be solved by the present method of mapping.

From the viewpoint of trajectory families, this problem amounts to the selection of a particular member from the two-terminal family, defined by $\mathbf{r}_1$ and $\mathbf{r}_2$, to satisfy the requirement $r_P = r_P^*$. Assuming $\mathbf{r}_1$ and $\mathbf{r}_2$ are noncollinear, the problem is a planar one. As seen in Sec. V, the O-locus of the two-terminal family is a straight line in the plane of motion defined by $\mathbf{r}_1$ and $\mathbf{r}_2$, and the O-locus of the family of trajectories satisfying the periapsis-radius constraint in this plane is a hyperbola. Consequently, the solution is given by the intersection of the O-line and the O-hyperbola. Let us first specify the sense of motion to be positive. The O loci of the two families in the v-plane are shown in Fig. 14. In the ξ,η system with origin at Q_1, the equations of the two loci, as found before, are

$$[(\sigma_P + 1)\xi - 1]^2 - \eta^2[(\sigma_P + 1)/(\sigma_P - 1)] = 1 \tag{F1}$$

for the O hyperbola and

$$\eta = \xi \cot\varphi_1 - \tan(\psi/2) \tag{H1}$$

for the O line. Here $\sigma_P = r_1/r_P^*$, and ψ and φ_1 are constants, defined in Fig. 14. Solving Eqs. (F1, H1) simultaneously yields

$$\xi = \frac{\sigma_P - 1 - \cot\varphi_1 \tan(\psi/2) \pm \sigma_P \sec(\psi/2)[(r_1 - r_P^*)(r_2 - r_P^*)/r_1r_2]^{1/2}}{\sigma_P^2 - \csc^2\varphi_1} \tag{17}$$

which confirms Roth's result, but in a simpler form. It enables one to see immediately that there are always two real roots under the hypothesis that r_P^* is no greater than r_1 or r_2, and that a double root arises when $r_P^* = r_1$ or r_2. However, it is important to note that neither Roth's original solution, nor its present form, Eq. (17), is necessarily the solution of the problem, since, as pointed out earlier in Sec. V, the unrealistic trajectories must be excluded. It follows that the solution point must satisfy the additional reality constraint

$$\xi > \xi_I^* \tag{18}$$

where ξ_I^* is the abscissa of the critical point O_I^* (Fig. 13). Thus the solution still can be unique or none despite the two roots being always real. Viewing geometrically in the v-plane, the solution points for the problem must lie on the

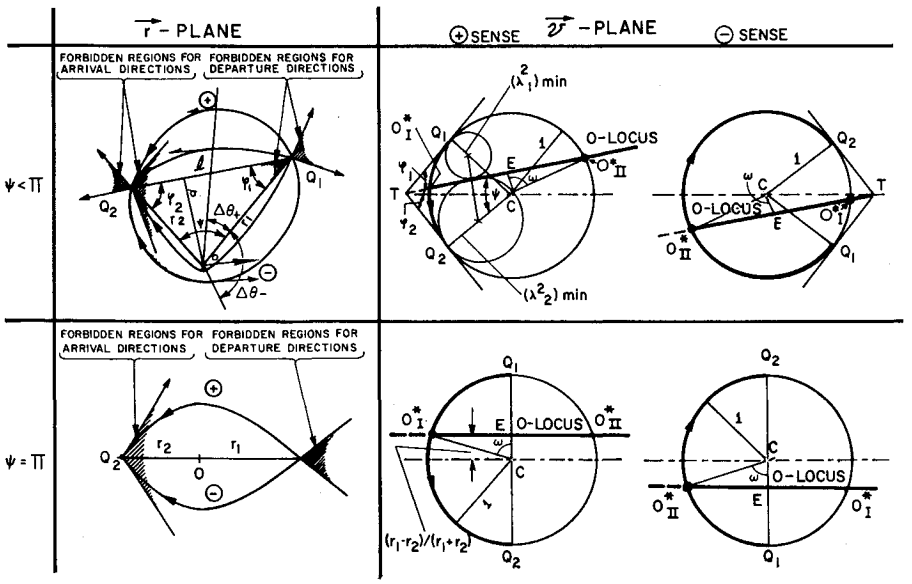

Fig. 13 The two-terminal family of Keplerian trajectories.

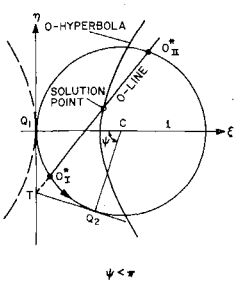

Fig. 14 Determination of two-terminal trajectory with specified periapsis radius.

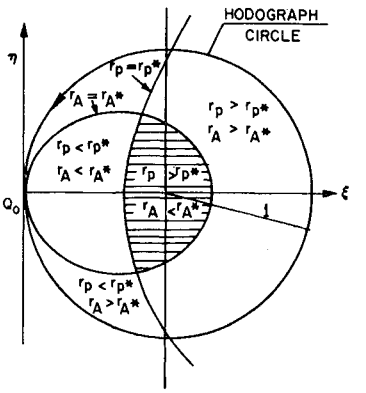

Fig. 15 Hodograph regions for families of Kepler orbits under inequality constraints.

realistic branch of the O-hyperbola, and the realistic portion of the O-line. Thus, there will be two, one, or no solution for the problem according as the two realistic portions of the O loci intersect in two, one, or no real points. If negative sense of motion is assumed, the treatment will be the same except the appropriate changes of signs, and that the reality constraint should refer to the critical point O_{II}^* instead of O_I^*.

The special case of $\psi = \pi$ will now be treated. We note here the orientation of the plane of motion is not determined, and to fix this plane, we may specify the vector $\mathbf{r}_P$ instead of merely its magnitude. Actually the hodograph geometry is simpler in this special case, as the O-line in any arbitrary plane of motion is now vertical, as given by

$$\xi = 2r_2/(r_1 + r_2) \tag{H2}$$

leaving η as the only variable. The solution for η is immediate from Eqs. (F1) and (H2) giving

$$\eta = \pm[2/r_P^*(r_1 + r_2)][r_1 r_2(r_1 - r_P^*)(r_2 - r_P^*)]^{1/2} \tag{19}$$

and the reality constraint is

$$\eta > \eta^* \tag{20}$$

where η^* is the ordinate of the critical point on the O-line, where $\eta < 0$. Formulas (19) and (20) hold for either sense of motion. Here again we see that the hypothesis $r_P^* \gtrless r_1$ or r_2 guarantees the two roots for η being real, and the hodograph geometry further shows that the two roots are both on the realistic branch of the O-hyperbola. However, the inequality constraint (20) may rule out one of them, but not both. Thus we may conclude that, for the 180° case, and in either sense of motion in any arbitrary plane containing $\mathbf{r}_1$ and $\mathbf{r}_2$, there is at least one, and at most two realistic solutions for the problem; and a double solution arises when $r_P^* = r_1$ or r_2, and this solution is realistic. It is to be noted that, in comparison with Roth's result, the present solution given by Eq. (19) does not seem to present any computational difficulties as he anticipated for the case $\psi = \pi$.

The treatment is now completed. This example fully illustrates that the use of the normalized hodographic mapping followed by the method of loci provides a simple and effective approach to the solution of the problem. It not only leads directly to the analytical solution, but also enables one to see clearly the applicability of the mathematical solution to the physical problem under various terminal conditions, to clarify some possible complications concerning the solution, and to safeguard against the pitfall of the unrealistic solutions, which might be overlooked in numerical work. Furthermore, once the solution point is located in the v-plane, the type of the solution trajectory and the principal parameters associated with it may be readily determined from the hodograph, either graphically or analytically, in accordance with the correlation formulas given in Sec. III and the Appendix in Ref. 10. However, such details will not be elaborated here.

Another example similar to this one is to determine a two-terminal trajectory under a specified maximum altitude constraint. In this problem, instead of an O-hyperbola, we have an O-ellipse in the v-plane, and the problem reduces to finding the intersection of this ellipse with the O-line. The treatment is essentially the same, and analytical solutions analogous to Eqs. (17) and (19) can be easily worked out.

Another class of trajectory problems which can be easily handled by the present method is the analysis of a class of trajectories whose principal parameters have predetermined upper and/or lower limits. For example, in mission planning, it is often desirable to keep the closest approach to a planet above a certain altitude r_{P^*} and at the same time, the farthest approach below a certain limit r_{A^*}. The totality of trajectories that are generated from a fixed burnout point and satisfy these requirements can be represented in the v-plane by the region bounded by the O-hyperbola with $r_P = r_{P^*}$, and the O-ellipse with $r_A = r_{A^*}$, as shown in Fig. 15. Once this hodographic region is mapped, the global characteristics of the family can be easily analyzed. If the plane of motion is not restricted, the composite planar region will generate a surface of revolution bounding a 3-dimensional region in the v-space.

Examples of this sort are numerous. Extensive presentation of such applications, however, is not intended in the limited space here.

VIII. Normalized Hodographic Maps

To facilitate the analytical treatment of trajectory problems, and to provide quick graphical solutions, a few normalized hodographic maps have been developed as shown in Fig. 16 a, b and c. Maps a and b consist of lines of constant trajectory parameters corresponding to the first seven basic trajectory families mapped in Sec. V. Map c shows the images of all two-terminal trajectory families with a common range angle, but varying distance ratio. With these maps, graphical solution of many trajectory problems can be quickly determined. Analytic solutions, if desired, may be obtained by resorting to the equations in Table 1, which represent the families of lines in the map. Again the use of these maps in practical problems cannot be illustrated here owing to the limited space.

IX. Final Remarks

1) As illustrated throughout the preceding section, the chief advantage of the normalized hodographic mapping lies in its great simplification of the geometry of a constrained trajectory family. For comparison purpose we recall that the constraining hodograph of a two-terminal family in the absolute velocity space ($\mathbf{V}$) is a hyperbola[4,6] for each terminal, but in the normalized velocity space (v) it reduces to a straight line. Thus, from a family of infinitely many Kepler conics of all three types to a pair of velocity hyperbolas is the simplification gained through the ordinary hodographic mapping, and from such a pair of hyperbolas to a single straight line is the further simplification contributed by the normalized hodographic mapping. Similar situations are found in other families. It can be proved in general that, a locus represented by an algebraic equation of $2m$ degree (m = a positive

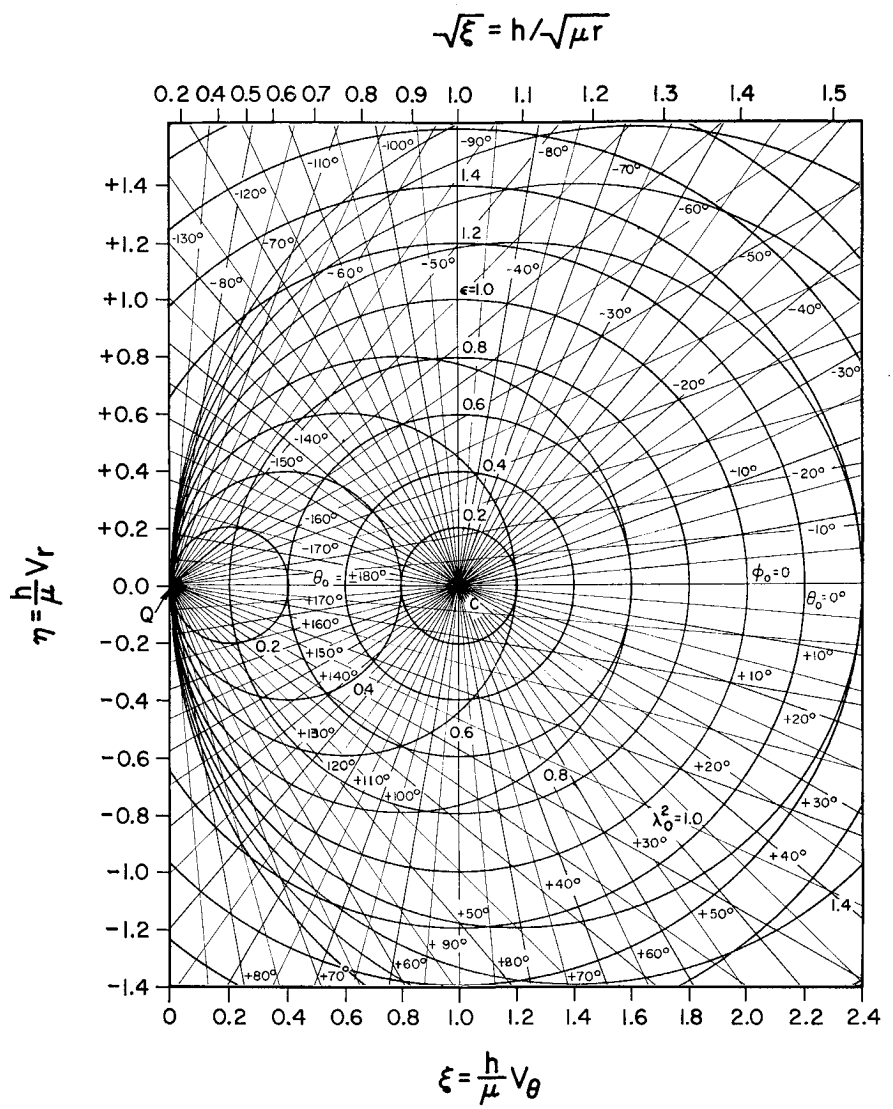

Fig. 16a The normalized hodographic map of Kepler orbits: lines of constant orbital parameters.

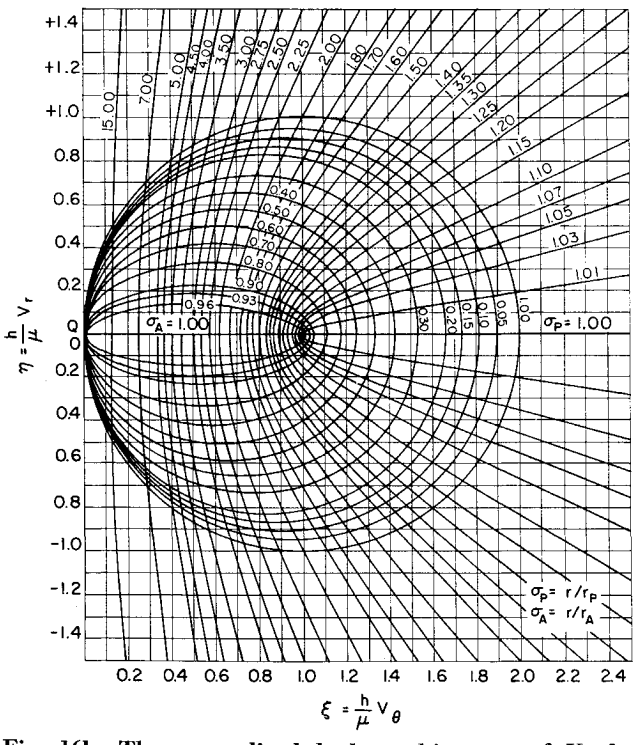

Fig. 16b The normalized hodographic map of Kepler orbits: lines of constant periapsidal and apoapsidal radii.

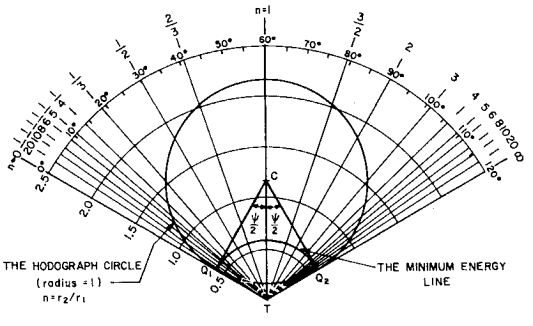

Fig. 16c The normalized hodographic map of the two-terminal families of Keplerian trajectories.

Table 1 The normalized hodograph of the families of constrained Keplerian trajectories (coterminal and unisense)

Family	Defined by	Geometry in $\dot{\mathbf{r}}$-space	O-locus in $\mathbf{v}$-space: Equation in ξ,η-coord		O-locus in $\mathbf{v}$-space: Description	Fig.	Remarks
A Isoangular-momentum 1) Planar 2) Spatial	 $\mathbf{h}$ = const h = const	Family of coterminal conics of same latus rectum	$\xi = h^2/\mu r_O$	(A1)	1) A straight line 2) A cylindrical surface	6	
B Isoenergetic 1) Planar 2) Spatial	k = const (λ_O = const)	Family of coterminal conics of the same type and same semi-major axis	$(\xi - \lambda_O{}^2)^2 + \eta^2 = \lambda^4{}_O$	(B1)	1) A circle 2) A circular torus	7	
C Cotangential	ϕ_O = const	Family of conics having a common tangent at the common terminal	$\eta + \xi \tan\phi_O = 0$	(C1)	A ray emanated from Q_O	8	Necessarily plana
D Isoeccentric 1) Planar 2) Spatial	ϵ = const	Family of coterminal similar conics	$(\xi - 1)^2 + \eta^2 = \epsilon^2$	(D1)	1) A circle 2) A spherical surface	9	
E Coaxial	θ_O = const	Family of coterminal conics of the same apsidal axis	$\eta = (1 - \xi)\tan\theta_O$	(E1)	A ray emanated from C	10	Necessarily planar (unless $\theta_O = 0$ or π)
F Equiperiapsis-radius 1) Planar 2) Spatial	r_P = const	Family of coterminal conics of the same periapsis radius	$[(\sigma_P + 1)\xi - 1]^2 - [(\sigma_P + 1)/(\sigma_P - 1)]\eta^2 = 1$ ($\sigma_P \equiv r_O/r_P > 1$)	(F1)	1) A branch of hyperbola 2) A hyperboloid of revolution	11	
G Equiapoapsis-radius 1) Planar 2) Spatial	r_A = const	Family of coterminal ellipses of the same apoapsis radius	$[(\sigma_A + 1)\xi - 1]^2 + [(1 + \sigma_A)/(1 - \sigma_A)]\eta^2 = 1$ ($\sigma_A \equiv r_O/r_A < 1$)	(G1)	1) An ellipse 2) An elliptic torus	12	
H Two-Terminal 1) $0 < \psi < \pi$ 2) $\psi = \pi$	$\mathbf{r}_1, \mathbf{r}_2$ = consts	Family of conics through 2 fixed points in space	$\eta = \xi\cot\varphi_1 - \tan(\psi/2)$ $\xi = 2r_2/(r_1 + r_2)$	(H1) (H2)	1) A straight line 2) A cylindrical surface	13	Origin of the ξ,η-system placed at Q_1; Eq. (H1) is for transfer angle $< \pi$.

integer) in the **V**-space will reduce to one of degree m in the $\mathbf{v}$-space, through such normalization.

2) As noted in Sec. III, the **O** locus of a Keplerian coterminal family also serves as its eccentricity indicatrix. Thus, each of the four linear loci found in Sec. V is expressing the law of linear eccentricity indicatrix for the trajectory family. Likewise, the laws of circular eccentricity indicatrix are found for the isoenergetic and isoeccentric planar families. Similar interpretations may be made for the other O loci. Under this role the O locus has its purely geometric significance, independent of the dynamics of motion, and the employment of such eccentricity indicatrix could be useful in the geometric study of conic families, just like the spherical indicatrix, and the Duppin indicatrix employed in differential geometry for the study of space curves. However, combining the eccentricity indicatrix with the unit circle and viewing them together as the hodograph image of the whole trajectory family yields dynamic information beyond that of purely geometric nature, and makes this method of mapping more valuable in the eyes of an orbital mechanician.

3) As a word of caution, the normalized hodograph does not give a direct comparison of the velocities referred to different origin points on the O locus unless they are of the same angular momentum. Hence the minimization of the characteristic velocity in an optimal impulsive maneuver problem cannot be treated in a straightforward manner in the $\mathbf{v}$-space like in the **V**-space.[9] However, when the family involved is of isoangular momentum, the treatment of such optimization by the present method of mapping is not only applicable, but also simple and direct.

4) Another kind of the orbital hodograph available for normalization is the polar version, in which the coordinate system is rotating with the orbiting mass instead of being fixed in the inertial space as the one employed in Hamilton's circular hodograph, which is the basis for the present mapping. Application of Eq. (1) to a polar orbital hodograph would result in a hodograph circle of fixed center location, but a radius equal to the orbital eccentricity instead of unity.[5,9] Hence to such a version, the principles and techniques developed here do not directly apply. Graphic work in the sense of normalized polar hodograph is found in Boksembom's work,[3] although no reference is made to his diagram as a hodographic representation in his original report. A brief discussion of this version is also found in Ref. 9 (p. 17).

5) In principle, the normalization of the velocity space in accordance with Eq. (1) is applicable to the motion in any central force field; and, in particular, the normalized circular hodograph applies equally well to an inverse square repulsive field although it is of no interest at present. As regards non-Keplerian motion, such as the satellite's motion under perturbation, or rocket flight under thrust, where the perturbed orbit or the powered trajectory may be viewed as the envelope of a family of osculating conics, the approach by the present method of mapping may also be advisable. However, the family is no longer coterminal, and special care must be taken in using the normalized hodograph. Such extended applications are yet to be developed.

References

[1] Hamilton, Sir W. R., "The Hodograph, or a New Method of Expressing in Symbolical Language the Newtonian Law of Attraction," *Proceedings of the Royal Irish Academy*, Vol. III, 1845-47, pp. 344–353.

[2] Woods, F. S., *Higher Geometry*, Ginn, Boston, Mass., 1922, pp. 127–130.

[3] Boksembom, A. S., "Graphical Trajectory Analysis," TN D-64, Dec. 1959, NASA.

[4] Stark, H. M., "Optimum Trajectories Between Two Terminals in Space," *ARS Journal*, Feb. 1961, pp. 261–263.

[5] Sun, F. T., "On the Hodograph Method for Solution of Orbit Problems," *Proceedings of the 12th International Astronautical Congress*, Academic Press, New York, 1963, pp. 879–915.

[6] Sun, F. T., "Hodograph Analysis of the Free-Flight Trajectories Between Two Arbitrary Terminal Points," CR-153, Jan. 1965, NASA.

[7] Altman, S. P., *Orbital Hodograph Analysis*, Science and Technology Series, Vol. 3, American Astronautical Society, 1965.

[8] Roth, H. L., "Determination of an Orbit Between Two Position Vectors with Specific Periapsis Radius," *Journal of the Astronautical Sciences*, Vol. 13, No. 5, Sept.-Oct. 1966.

[9] Sun, F. T., "On the Use of Hodographic Mapping in Trajectory Analysis," PM-82, June 1969, NASA, Electronic Research Center, Cambridge, Mass.

[10] Sun, F. T., "On the Normalized Hodographic Mapping for the Constrained Trajectory Families," AIAA Paper 69-924, Princeton, N. J., 1969.

FEBRUARY 1971 AIAA JOURNAL VOL. 9, NO. 2

Effect of Crew Motions on Spacecraft Orientation

JOHN R. DAVIDSON*
NASA Langley Research Center, Hampton, Va.

AND

ROBERT L. ARMSTRONG†
Dynatech R/D Co., Cambridge, Mass.

Crew motions can affect the angular orientation of a spacecraft. Such motions are somewhat random and must be treated stochastically. Linearized equations of motion for the spacecraft are solved to obtain a simple relationship between individual crew motions and the angular change in spacecraft orientation. The additive effect of many motions is found by treating the problem as a Markovian random walk. Starting from a known distribution of crew motions, the mean waiting time required to reach predetermined maximum allowable angular deviations is found; the inverse of the waiting time can then be used to determine the frequency of control jet firing and fuel consumption rate. For heavy spacecraft, where many individual motions occur between jet firings, the diffusion equation applies. For smaller spacecraft, motions are treated as discrete steps using matrix equations.

Nomenclature

a = variance of the angular rate of change
B = number of subperiods of length h
b = mean angular rate of change
$E(\ )$ = expectation
H = angular momentum
h = length of subperiods
I = inertia
I = unit matrix
K = reduced mass
M = mass of spacecraft
m = internal moving point mass
P = probability that an event will occur
$\bar{P}$ = transition matrix
p = Laplace transform parameter (angle)
$\bar{p}$ = one-step transition matrix
$\hat{p}$ = modified one-step transition matrix (reflecting boundaries)
$\bar{r}_1$ = position vector of mass m in X, Y, Z coordinates
$\bar{r}_2$ = position vector of differential mass dM in X, Y, Z coordinates
S = surface bounded by the path of m
s = Laplace transform parameter (time)
T,t,τ = time
u = probability density function for X (angle)
Var = variance
W = waiting time
X = angle of rotation
δ_{ij} = Kronecker delta
η = to be defined by Eq. (58)
λ = number of moves/sec
$\tilde{\lambda}$ = matrix of λ's
μ = mean number of moves, $\mu = \lambda T$
ν = probability vector
$\bar{\rho}$ = position vector of mass m in (1), (2), (3) coordinate system
$\bar{\rho}_M$ = position vector of differential mass dM in (1), (2), (3) coordinate system
φ = angle of rotation
ω = angular velocity

Subscripts

i,j,k,l,N = indices
b = upper boundary for diffusion analysis
c = center of mass
0 = nominal position; or boundary value of λ
r = relative to moving coordinates
γ = upper boundary state for discrete-step analysis

Received March 2, 1970; revision received July 29, 1970.
* Aerospace Engineer. Member AIAA.
† Principal Engineer.

Introduction

SINCE space flight has become a practical accomplishment there has been an increased interest in the motion of bodies in a reduced force, or zero force environment. This is because, at large distances from the earth, gravitational-gradient torques and atmospheric drag have a diminishing influence on spacecraft motion. There, the major spacecraft torques originate internally and are caused by the crew and